ELECTROCHEMISTRY

Hierarchical MoS$_2$ tubular structures internally wired by carbon nanotubes as a highly stable anode material for lithium-ion batteries

Yu Ming Chen,[1]* Xin Yao Yu,[2]* Zhen Li,[1] Ungyu Paik,[2] Xiong Wen (David) Lou[1]†

Molybdenum disulfide (MoS$_2$), a typical two-dimensional material, is a promising anode material for lithium-ion batteries because it has three times the theoretical capacity of graphite. The main challenges associated with MoS$_2$ anodes are the structural degradation and the low rate capability caused by the low intrinsic electric conductivity and large strain upon cycling. Here, we design hierarchical MoS$_2$ tubular structures internally wired by carbon nanotubes (CNTs) to tackle these problems. These porous MoS$_2$ tubular structures are constructed from building blocks of ultrathin nanosheets, which are believed to benefit the electrochemical reactions. Benefiting from the unique structural and compositional characteristics, these CNT-wired MoS$_2$ tubular structures deliver a very high specific capacity of ~1320 mAh g^{-1} at a current density of 0.1 A g^{-1}, exceptional rate capability, and an ultralong cycle life of up to 1000 cycles. This work may inspire new ideas for constructing high-performance electrodes for electrochemical energy storage.

INTRODUCTION

Lithium-ion batteries (LIBs) have been widely used in consumer electronics (1, 2). However, the rapidly growing demand for electric vehicles, hybrid electric vehicles, and large-scale electric grid energy storage has triggered an urgent pursuit for advanced batteries with much higher energy density (3, 4). Metal sulfides represent an interesting class of electrode materials for LIBs because of their high abundance, low cost, and intriguing properties (5–13). Among them, molybdenum disulfide (MoS$_2$), a typical two-dimensional (2D) material, has been considered as a promising anode material for LIBs because of its high specific capacity from a four-electron transfer per formula unit (11–13). However, like many other electrode materials, MoS$_2$-based anodes are plagued with two main challenges that cause low rate capability and fast capacity decay: the low intrinsic electric conductivity and the large strain upon cycling (14). To tackle these challenges, two typical strategies have been exploited to improve the electrochemical performance of MoS$_2$-based electrodes. One is to synthesize nanostructured MoS$_2$ materials that can relax the strain upon cycling, therefore maintaining the structural stability and decreasing the barrier for lithium intercalation (12). The other is to grow the poorly conductive MoS$_2$ on carbonaceous supports, such as graphene, to improve the electron and ion transport (11, 14–16). In particular, one-dimensional (1D) carbon-MoS$_2$ nanocomposites have been studied in view of their enhanced ion and electron transport property (13, 17–20). However, two major constraints remain in these carbon-MoS$_2$ nanocomposites. First, the electrolyte needs to diffuse through the surface of carbon materials to react with the MoS$_2$ underneath, thus limiting the rate capability of the electrode (11). In addition, these nanocomposites usually contain a significant amount (>30 wt %) of barely active carbon materials, which not only decreases the mass loading of MoS$_2$ but also more seriously overconfines the electrodes,

thus causing mechanical strain again (13, 14). Thus, it is highly desirable to develop a better 1D structure of the MoS$_2$/carbon composite with high specific capacity and excellent cycling stability.

Here, we design a novel strategy to synthesize porous hierarchical MoS$_2$ tubular structures constructed from ultrathin nanosheets and wire the interior of these tubular structures with aligned carbon nanotubes (CNTs) to enhance the electric conductivity. The overall synthesis approach involves the following steps, as schematically shown in Fig. 1. First, carboxylic groups are introduced onto multiwalled CNTs (fig. S1) by refluxing the CNTs in acid. The CNTs are then embedded into polyacrylonitrile (PAN) nanofibers by an electrospinning method (Fig. 1A) (21). The abundant –CN functional groups in PAN could coordinate with the carboxylic acid groups on CNTs, forming a good/homogeneous mixture. During the electrospinning process, the CNTs align along the streamlines of the electrospinning solution owing to the elongation and surface tension of the fluid jet (22, 23). As a result, a flexible tube-in-fiber structure with CNTs aligned in PAN fibers is obtained. A protective layer of CoS$_x$ is grown onto the CNT/PAN tube-in-fiber composite by a combined precipitation and sulfidation process to prevent the damage of structure during the synthesis process and maintain the 1D morphology of the final materials (Fig. 1, B and I, and fig. S2). Next, a facile hydrothermal approach is used to grow ultrathin MoS$_2$ nanosheets on the composite and completely remove the PAN simultaneously, forming the tubular MoS$_2$ structure (Fig. 1B, II). Then, the composite is heated in N$_2$ (95%)/H$_2$ (5%) at 800°C for 2 hours to increase the crystallinity of MoS$_2$. Meanwhile, the protective layer of CoS$_x$ is reduced to form Co nanoparticles (Fig. 1B, III) (24, 25). Finally, the Co nanoparticles are dissolved by acid treatment, thus generating some pores on the wall of MoS$_2$ nanotubes, to obtain CNT-wired porous hierarchical MoS$_2$ nanotubes consisting of ultrathin nanosheets (Fig. 1B, IV). As expected, the CNT-wired MoS$_2$ hierarchical tubular structures exhibit remarkable electrochemical performance with high specific capacity, outstanding rate capability, and an ultralong cycle life when evaluated as an anode material for LIBs.

[1]School of Chemical and Biomedical Engineering, Nanyang Technological University, 62 Nanyang Drive, Singapore 637459, Singapore. [2]World Class University (WCU) Department of Energy Engineering, Hanyang University, Seoul 133-791, Korea.
*These authors contributed equally to this work.
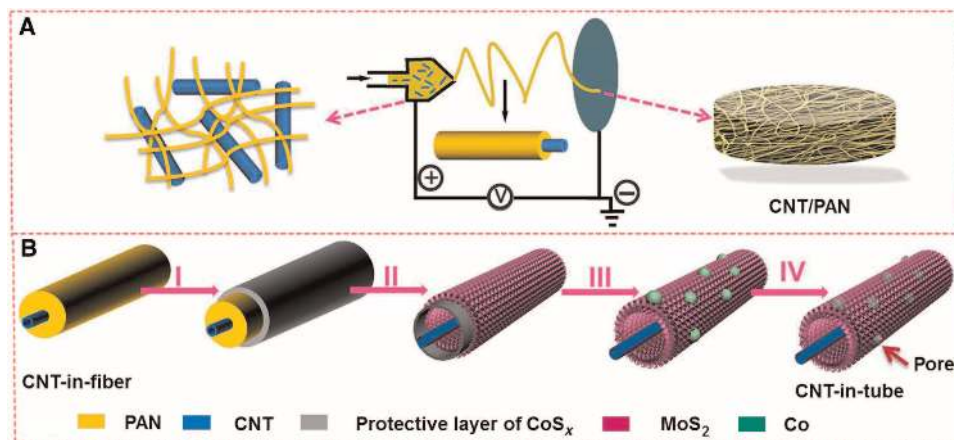†Corresponding author. Email: xwlou@ntu.edu.sg

Fig. 1. Schematic illustration of the synthesis of the CNT-wired hierarchical MoS₂ tubular structures constructed from ultrathin nanosheets (CNT/MoS₂ nanohybrid). (A) Illustration of the synthesis process of the CNT/PAN tube-in-fiber structure by electrospinning. **(B)** Schematic of the fabrication process for the CNT-in-tube structure. (I) Growth of a protective layer of CoS_x on the CNT-in-fiber composite. (II) Formation of MoS_2 nanosheets on the composite accompanied by the removal of PAN, yielding a tubular structure. (III) Heating treatment of the hybrid to reduce the CoS_x to Co nanoparticles. (IV) Acid treatment to remove Co particles to obtain a CNT/MoS₂ tubular structure.

RESULTS

Synthesis and characterizations of CNT-wired hierarchical MoS₂ tubular structures (CNT/MoS₂ hybrids)

Figure 2A shows a typical field-emission scanning electron microscopy (FESEM) image of the CNT/PAN composite nanofiber with a smooth surface and a diameter of ~200 nm. The transmission electron microscopy (TEM) image shown in Fig. 2B confirms a tube-in-fiber structure with a single CNT well aligned along the axis of the nanofiber. The surface of the nanofibers becomes rougher after refluxing in the ethanol solution of $(CH_3COO)_2Co·4H_2O$ (fig. S3), suggesting the successful deposition of Co acetate hydroxide with a tetragonal phase (26), as confirmed by powder x-ray diffraction (XRD) (fig. S4). The easy deposition of Co acetate hydroxide onto the tube-in-fiber composite could be mainly ascribed to the existence of abundant –CN functional groups in PAN. After sulfidation treatment in thioacetamide (TAA) solution, the outer layer of Co acetate hydroxide can be transformed to CoS_x as a protective layer, whereas the 1D morphology is perfectly retained (Fig. 2C). The well-defined CoS_x layer on the surface of the CNT/PAN nanofiber can be easily identified (Fig. 2D). Energy-dispersive x-ray spectroscopy (EDX) and XRD results show that the shell mainly consists of amorphous CoS_x (figs. S5 and S6I). After a facile hydrothermal process, the surface of the composite is uniformly covered with MoS_2 nanosheets (Fig. 2E). This process is accompanied by complete removal of PAN, leading to the formation of the tubular structure. In addition, the CNTs remain well aligned in the core, yielding an interesting CNT-in-tube structure (Fig. 2, F and G). The as-synthesized CNT/MoS₂-CoS_x hollow structures are further annealed to increase the crystallinity of MoS_2 (fig. S6II). FESEM (Fig. 2H) and TEM (Fig. 2I) images show that the 1D hollow morphology is well maintained, with negligible size change after annealing. Some particles can be observed on the wall of MoS_2 nanotubes (Fig. 2I). High-resolution TEM (HRTEM) analysis reveals that they have an interplanar distance of 0.205 nm corresponding to the Co (111) plane, suggesting that the CoS_x layer has been reduced into

Co nanoparticles during the annealing process. XRD analysis (fig. S6III) shows two sets of diffraction peaks that can be assigned to the hexagonal MoS_2 and Co [Joint Committee on Powder Diffraction Standards (JCPDS) card nos. 37-1492 and 15-0806].

The Co nanoparticles are removed by acid treatment to generate some pores on the wall of MoS_2 tubular structures without affecting the overall morphology of the CNT/MoS₂ nanohybrid (Fig. 3A). The crystallographic structure and phase purity of the nanohybrid are characterized by XRD (Fig. 3B). All the diffraction peaks can be perfectly indexed to the hexagonal MoS_2 (JCPDS card no. 37-1492) with no residues or impurity phase. The composition of the nanohybrid is further examined by EDX (Fig. 3C). The Mo/S atomic ratio of the hybrid is determined to be around 1:1.87, which is close to the stoichiometric composition. It also confirms that the Co particles have been completely removed after the acid treatment compared to the EDX spectrum before the acid treatment (fig. S7). Figure 3 (D and E) shows that a single CNT with a diameter of ~35 nm aligns with the axis of MoS_2 tubular structures and attaches to the inner wall of the tubular structure. In addition, the wall of the MoS_2 tubular structures is about 70 nm thick. A closer examination (Fig. 3, F and G) reveals that the MoS_2 nanosheets are 1.1 to 3.3 nm thick, corresponding to only two to five layers of MoS_2. X-ray photoelectron spectroscopy (XPS) study demonstrates the existence of Mo, S, and C in the prepared materials (fig. S8A). The binding energies at 229.4 and 232.5 eV in the Mo 3d–S 2s spectrum are ascribed to Mo $2d_{5/2}$ and Mo $2d_{3/2}$, confirming the chemical state of Mo^{4+} in MoS_2 (fig. S8B). The binding energies of S $2p_{3/2}$ and S $2p_{1/2}$ bands are located at 162.2 and 163.3 eV, respectively, which are due to the S^{2-} state in MoS_2 (fig. S8C). The high-resolution XPS spectrum of C 1s further confirms that the synthesized materials contain CNTs (fig. S8D) (27–31). The CNT content in the as-synthesized 1D CNT/MoS₂ hollow nanohybrid is determined to be about 10.7 wt % (fig. S9). With the hollow tubular structure and ultrathin nanosheets, the CNT/MoS₂ nanohybrids show a high surface area of ~200 m² g⁻¹, with the pore sizes mostly below 25 nm (fig. S10).

Without the introduction of CNTs, similar hierarchical MoS_2 tubular structures can be obtained (figs. S11 and S12), and irregular MoS_2
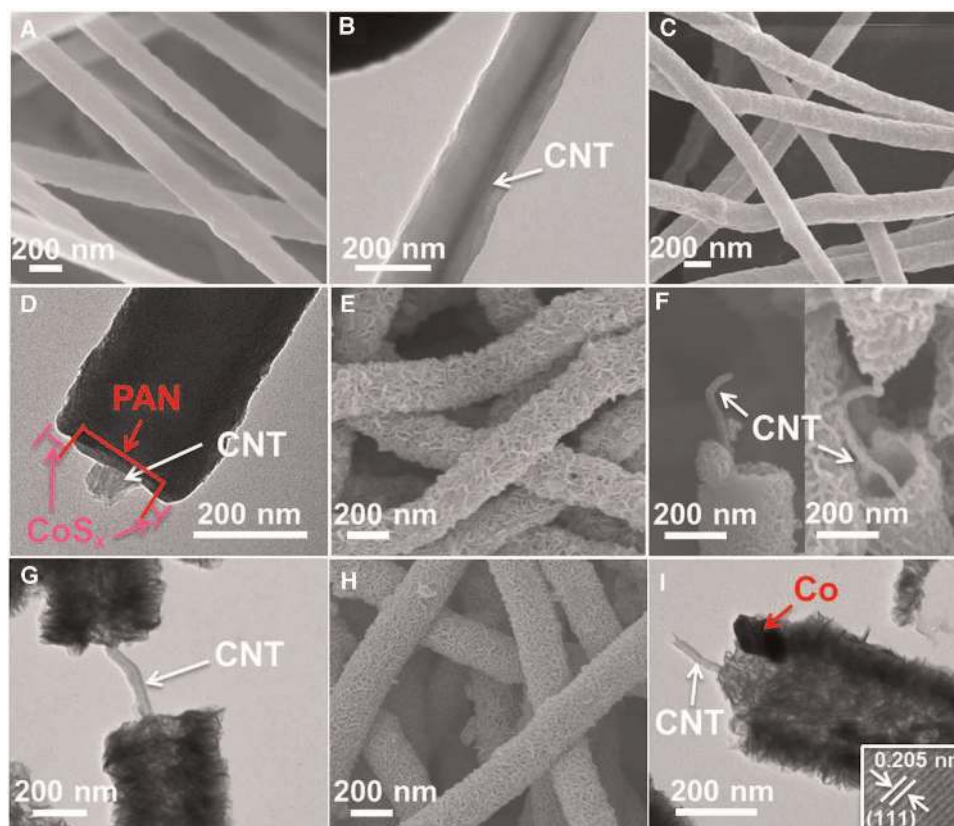
Fig. 2. Structural characterizations of the intermediate products. (**A** to **I**) FESEM, TEM, and HRTEM images of the CNT-in-PAN nanofibers (A and B), the CNT/PAN-CoS$_x$ nanofibers (C and D), the CNT/MoS$_2$-CoS$_x$ tubular structures (E to G), and the CNT/MoS$_2$-Co tubular structures (H and I).
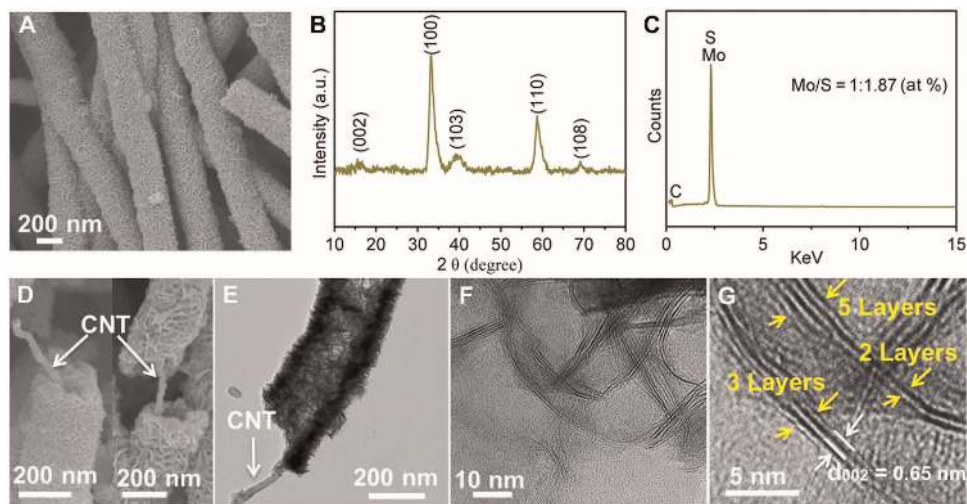

Fig. 3. Characterizations of the CNT/MoS$_2$ tubular nanohybrid. (**A**) FESEM image. (**B**) XRD pattern. a.u., arbitrary units. (**C**) EDX spectrum. at %, atomic percent. (**D**) FESEM image. (**E** and **F**) TEM images. (**G**) HRTEM image.

flakes are synthesized under the same hydrothermal conditions in the absence of any templates (fig. S13). The thickness of the MoS_2 shell that is wired (or not wired) by CNTs can be easily controlled by varying the concentration of the Mo precursor in the synthesis solution (figs. S14 and S15). The type of CNTs can also be varied inside MoS_2 tubular structures. For example, CNTs with a smaller diameter of ~15 nm can be similarly aligned inside the MoS_2 shell (fig. S16). The number of CNTs in each MoS_2 tubular structure can be systematically controlled by altering the amount of CNTs in the PAN matrix. As shown in Fig. 4 (A to C), two strands of CNTs can be clearly observed in a single MoS_2 tubular structure. The number of CNTs aligned in a single MoS_2 tubular structure can be controlled to be predominantly three (Fig. 4, D to F) or even four (Fig. 4, G to I). All these results show that the designed strategy is highly effective.

Electrochemical evaluation of the hollow nanohybrids

The CNT/MoS_2 nanohybrid is evaluated as an anode material for LIBs, demonstrating its promising application. Figure 5A shows typical galvanostatic charge-discharge voltage profiles of the hybrid in the voltage range of 0 to 3 V versus Li/Li$^+$ at a current density of 0.1 A g^{-1}. Two voltage plateaus located at 1.1 and 0.7 V can be clearly seen in the first discharge process, which can be attributed to the insertion of Li$^+$ into the interlayer lattice of MoS_2 to form Li$_x$$MoS_2$ and a conversion reaction

process between Li$_x$$MoS_2$ and Li$^+$, respectively (32–34). A pronounced peak at around 2.3 V can be assigned to the delithiation of Li$_2$S to S in the first charge process. A different discharge profile with two voltage plateaus located at ~1.9 and 1.3 V is observed in the following discharge process, suggesting a multistep lithium insertion mechanism after the first cycle (19, 35, 36). Typical cyclic voltammograms of the nanohybrid with representative cathodic/anodic peaks (fig. S17A) are in agreement with the above charge-discharge profiles. From Fig. 5A, the first reversible capacity of the CNT/MoS_2 hollow nanohybrid is 1320 mAh g^{-1}, which is much higher than that of MoS_2 nanotubes (1150 mAh g^{-1}; fig. S17D) and MoS_2 flakes (750 mAh g^{-1}; fig. S18). The irreversible capacity of 531 mAh g^{-1} in the first cycle corresponding to a Coulombic efficiency of 71.3% could be due to some irreversible processes, such as the formation of the solid-electrolyte interface film and the decomposition of electrolyte (37–39).

The cycling performance of the CNT/MoS_2 nanohybrid electrode is presented in Fig. 5 (B and C). As shown in Fig. 5B, the CNT/MoS_2 nanohybrid electrode delivers a reversible specific capacity of ~1100 mAh g^{-1} at 0.5 A g^{-1} with no significant decay of capacity after 200 cycles. On the other hand, the MoS_2 nanotube electrode exhibits a lower specific capacity of around 870 mAh g^{-1} (fig. S17E). Both CNT/MoS_2 and MoS_2 tubular structures show greatly enhanced lithium storage performance as compared with the MoS_2 flake electrode (fig. S18). As shown in the
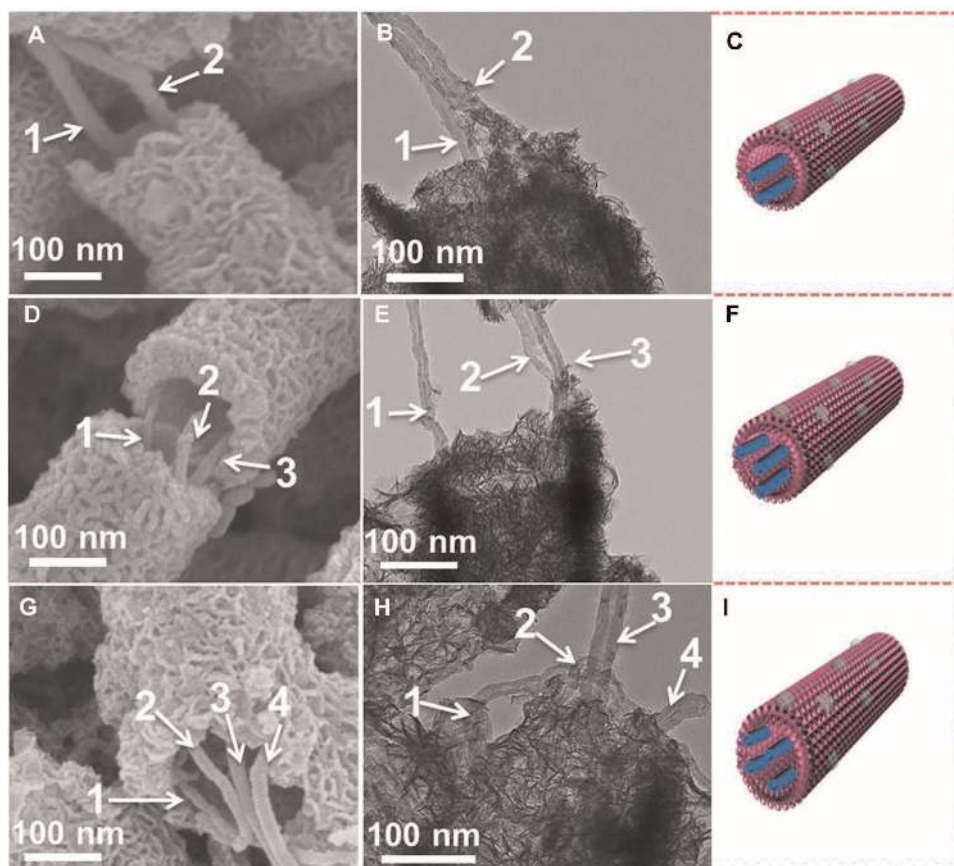
Fig. 4. Control of the number of CNTs in the CNT/MoS₂ tubular nanohybrids. (**A** to **I**) FESEM (A, D, and G) and TEM images (B, E, and H) and schematics (C, F, and I) of the CNT/MoS_2 tubular structures with different numbers of CNTs. Double (A to C), triple (D to F), and quadruple (G to I) CNTs in each MoS_2 tubular structure are shown.
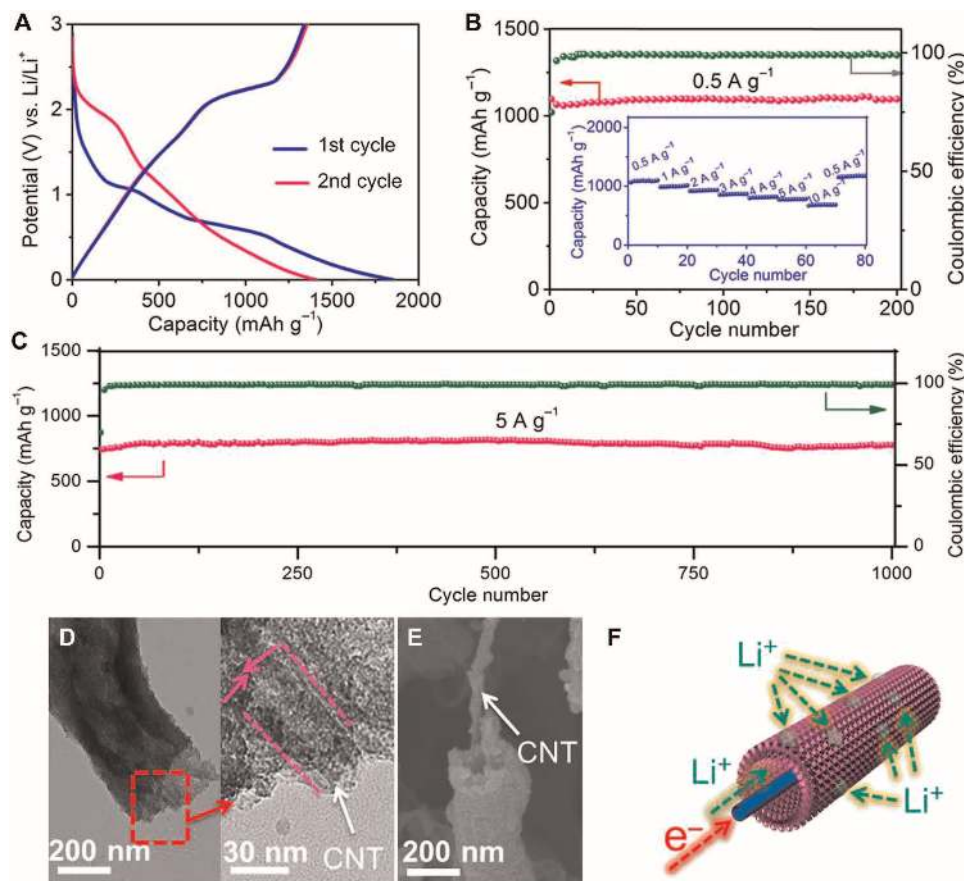
Fig. 5. Electrochemical performance of the CNT/MoS₂ tubular nanohybrid. (**A**) Charge-discharge voltage profiles at 0.1 A g⁻¹. (**B**) Cycling performance at 0.5 A g⁻¹ and rate capability test (inset) for CNT/MoS₂. (**C**) Cycling performance at 5 A g⁻¹ for 1000 cycles. (**D** and **E**) TEM (D) and FESEM (E) images of the CNT/MoS₂ structure after cycling for 200 cycles. (**F**) Schematic of transport paths for Li⁺ ions and electrons in the CNT/MoS₂ tubular structure.

inset of Fig. 5B, this CNT/MoS₂ hybrid electrode also shows exceptional rate capability. At current densities of 0.5, 1, 2, 3, 4, 5, and 10 A g⁻¹, the reversible capacities of the CNT/MoS₂ nanohybrid are ~1115, 1000, 926, 867, 815, 776, and 670 mAh g⁻¹, respectively. When the current density is reduced back to 0.5 A g⁻¹ from 10 A g⁻¹, a high capacity of 1145 mAh g⁻¹ can be immediately resumed. Moreover, the CNT/MoS₂ hybrid electrode also shows excellent cycling stability at a very high current density of 5 A g⁻¹ (Fig. 5C). A remarkably reversible capacity of ~800 mAh g⁻¹ can be retained even after 1000 cycles. The Coulombic efficiency at both low and high current densities for the CNT/MoS₂ and MoS₂ electrodes is nearly 100% after the first few cycles (Fig. 5, B and C, and fig. S17B). To investigate the structural stability of the materials, we carried out a postmortem study by FESEM and TEM examinations. Clearly, the size, shape, and structural integrity of both the 1D CNT/MoS₂ nanohybrid (Fig. 5, D and E, and fig. S19) and the MoS₂ nanotube (fig. S20) are still well retained, with only some changes in the MoS₂ nanosheets. Meanwhile, the MoS₂ flakes suffer from great structural degradation after cycling (fig. S21). These results demonstrate the great structural advantages of such 1D tubular structures. Electrochemical impedance spectroscopy (fig. S22) analysis shows that the CNT/MoS₂ hybrid manifests the lowest charge transfer resistance for Li⁺-ion insertion and extraction

(*40*). Furthermore, the resistance of the prepared nanohybrid is lower than that of other MoS₂/carbon composite electrodes (table S1).

DISCUSSION

The designed strategy for synthesizing the CNT/MoS₂ tubular nanohybrids presented in this work is facile and easily reproducible. The simple electrospinning synthesis of a 1D tube-in-fiber structure with aligned CNTs produces a novel template. This provides an alternative route for preparing functional tubular materials internally wired by CNTs. The introduction of the protective CoS$_x$ layer onto the surface of polymeric fibers overcomes the inherent disadvantages of polymer templates, such as low stability under harsh conditions, to maintain the 1D morphology of the material during the hydrothermal process. In addition, such a protective layer serves as a sacrificial component to produce pores on the wall of MoS₂ nanotubes in the final products. The polymer adopted in this work can be simply removed during the MoS₂ deposition process to create the tubular structure. Several important parameters that influence the electrochemical properties of the hybrids, including the thickness of MoS₂ shells, the type of CNTs,

and the number of CNTs in each MoS_2 tubular structure, can be well controlled by altering their corresponding precursors in the starting materials.

By virtue of the unique tubular structure, the 1D CNT/MoS_2 nanohybrid exhibits exceptional electrochemical performance as the anode for LIBs. To the best of our knowledge, the performance of this nanohybrid is significantly better than that of other MoS_2-based anodes (table S2). The superior performance of our CNT/MoS_2 tubular nanohybrid might be due to the following aspects, as illustrated in Fig. 5F. First, the good organization of ultrathin MoS_2 nanosheets and the 1D porous tubular structure enable a short diffusion distance for fast Li^+-ion diffusion, stable structural integrity that effectively buffers the mechanical stress during the charge-discharge process, and a sufficiently large electrode/electrolyte interface for the rapid charge transfer reaction (41–43). Second, both the MoS_2 nanotubes and the interior CNTs can act as channels for electron transport (44, 45). Third, the CNTs not only serve as a conductive path but also help to enhance the structural stability of the overall electrode during the lithiation/delithiation process (13).

In summary, we report an original strategy for synthesizing an interesting tubular nanohybrid of porous MoS_2 nanotubes constructed from ultrathin nanosheets wired by CNTs. This strategy relies on the successful alignment of CNTs in electrospun polymeric nanofibers. The various important factors that influence the electrochemical performance of the electrode, such as the shell thickness of MoS_2 tubular structures and the number of CNTs inside each MoS_2 tubular structure, can be systematically adjusted. Benefiting from the advantageous structure, the CNT/MoS_2 tubular nanohybrid exhibits remarkable electrochemical performance as anode materials in LIBs with a very high specific capacity of up to 1300 mAh g^{-1}, outstanding rate capability, and an ultralong cycle life of up to 1000 cycles. Such a strategy could be readily extended to other materials for the development of high-performance electrodes for better LIBs.

MATERIALS AND METHODS

Synthesis of the CNT/PAN tube-in-fiber composite
The mixture solution was prepared by adding 1.5 g of PAN (Sigma-Aldrich) and a certain amount of functionalized CNTs (obtained by reflux in HNO_3 at 80°C for 1 hour) in 19 ml of dimethylformamide (Sigma-Aldrich) solvent. The applied working voltage, flow rate, and distance between the needle and the collector were fixed at 13 kV, 0.04 mm min^{-1}, and 16 cm, respectively.

Synthesis of a protective layer of CoS_x onto the CNT/PAN tube-in-fiber composite
Cobalt acetate tetrahydrate (0.774 g) (Sigma-Aldrich) was dissolved in 100 ml of ethanol, followed by the addition of 100 mg of the as-prepared CNT/PAN tube-in-fiber composite into the solution. After sonication for 20 min, the above mixture was heated to 80°C in an oil bath for several hours to grow Co acetate hydroxide onto the CNT/PAN composite. The obtained CNT/PAN-Co acetate hydroxide composite and 0.13 g of TAA (Sigma-Aldrich) were dispersed in 40 ml of ethanol, transferred to a 100-ml Teflon-lined stainless steel autoclave, and then heated to 120°C for 12 hours to obtain the CNT/PAN-CoS_x composite.

Synthesis of the hierarchical MoS_2 tubular structures wired by CNTs (CNT/MoS_2 nanohybrids)
In a typical process, 25 mg of the prepared CNT/PAN-CoS_x composite was dispersed in 25 ml of water containing glucose (0.1 g), sodium molybdate ($Na_2MoO_4 \cdot 2H_2O$, 0.1 g), and thiourea (0.2 g). The mixture was transferred to a Teflon-lined stainless steel autoclave and kept in an electric oven at 220°C for 24 hours. After cooling to room temperature, the black precipitate of CNT/MoS_2-CoS_x was collected, washed with ethanol, and dried in an oven at 60°C. The collected precipitate was further annealed in N_2 (95%)/H_2 (5%) at 800°C for 2 hours, with a heating rate of 1°C min^{-1} to increase the crystallinity of MoS_2 and reduce the CoS_x layer to form Co nanoparticles. The obtained CNT/MoS_2-Co hollow nanohybrid was further treated with HCl to remove the Co nanoparticles to yield the nanohybrid of hierarchical porous MoS_2 nanotubes wired by CNTs. The thickness of the PAN layer, which translates to the diameter of MoS_2 tubular structures, can be controlled by changing the electrospinning conditions, such as the viscosity of the electrospinning solution and the applied working voltage. Porous MoS_2 tubular structures and MoS_2 flakes can also be prepared through a similar route without the addition of CNTs in the PAN matrix and fibrous composite precursors in the starting materials, respectively.

Materials characterization
The materials were characterized by TEM (JEOL, JEM-2010), HRTEM, FESEM (JEOL-6700), XRD (Bruker D2), thermogravimetric analysis (TGA), EDX (Oxford Instruments), and XPS (PHI5600). The nitrogen sorption measurement of the prepared composites was conducted by Autosorb 6B at 77 K.

Electrochemical measurements
The electrochemical tests were evaluated by cycling two-electrode 2032 coin cells with lithium foil as the counter/reference electrode, a Celgard 2400 film as the separator, and the mixed slurry consisting of the prepared CNT/MoS_2 structure, carbon black, and polyvinylidene difluoride in a 70:20:10 weight ratio on copper foil as the working electrode. The CNT/MoS_2 composite electrodes were pressed before assembling into coin cells. The loading density, diameter, and thickness of the prepared electrodes were ~1 mg cm^2, ~13 mm, and ~60 to 80 μm, respectively. The electrolyte was a 1 M $LiPF_6$ in a 50:50 (w/w) mixture of ethylene carbonate and diethyl carbonate. The charge-discharge tests were performed on a LAND battery tester at several current densities between the cutoff potentials of 0 and 3 V. Cyclic voltammetry and electrochemical impedance spectroscopy were conducted with a CHI 660C electrochemical workstation.

SUPPLEMENTARY MATERIALS
Supplementary material for this article is available at http://advances.sciencemag.org/cgi/content/full/2/7/e1600021/DC1

fig. S1. Characterizations of the CNTs.
fig. S2. FESEM images of the MoS_2 material synthesized by the hydrothermal method, with the addition of PAN nanofibers without the CoS_x protective layer.
fig. S3. FESEM images of the CNT/PAN-Co precursor composite nanofibers.
fig. S4. XRD pattern of the CNT/PAN-Co precursor.
fig. S5. EDX spectrum of the PAN/CNT-CoS_x composite nanofibers.
fig. S6. XRD analysis of the as-prepared materials.
fig. S7. EDX spectrum of the CNT/MoS_2-Co composite.
fig. S8. XPS spectra of the CNT/MoS_2 tubular nanohybrids.
fig. S9. TGA curves of CNTs, MoS_2 tubular structures, and CNT/MoS_2 nanohybrid in air.
fig. S10. N_2 sorption analysis of the CNT/MoS_2 tubular nanohybrids.

Chen et al. Sci. Adv. 2016;2:e1600021   13 July 2016

6 of 8

REFERENCES AND NOTES

1. M. Armand, J.-M. Tarascon, Building better batteries. *Nature* **451**, 652–657 (2008).

2. J.-M. Tarascon, M. Armand, Issues and challenges facing rechargeable lithium batteries. *Nature* **414**, 359–367 (2001).

3. J. B. Goodenough, K.-S. Park, The Li-ion rechargeable battery: A perspective. *J. Am. Chem. Soc.* **135**, 1167–1176 (2013).

4. Y. M. Chen, X. Li, K. Park, J. Song, J. Hong, L. Zhou, Y.-W. Mai, H. Huang, J. B. Goodenough, Hollow carbon-nanotube/carbon-nanofiber hybrid anodes for Li-ion batteries. *J. Am. Chem. Soc.* **135**, 16280–16283 (2013).

5. C. Y. Zhao, X. Wang, J. Kong, J. M. Ang, P. S. Lee, Z. Liu, X. Lu, Self-assembly-induced alternately stacked single-layer MoS₂ and N-doped graphene: A novel van der Waals heterostructure for lithium-ion batteries. *ACS Appl. Mater. Interfaces* **8**, 2372–2379 (2016).

6. X.-Y. Yu, L. Yu, L. Shen, X. Song, H. Chen, X. W. Lou, General formation of MS (M = Ni, Cu, Mn) box-in-box hollow structures with enhanced pseudocapacitive properties. *Adv. Funct. Mater.* **24**, 7440–7446 (2014).

7. X.-Y. Yu, L. Yu, H. B. Wu, X. W. Lou, Formation of nickel sulfide nanoframes from metal–organic frameworks with enhanced pseudocapacitive and electrocatalytic properties. *Angew. Chem. Int. Ed.* **127**, 5421–5425 (2015).

8. L. Yu, L. Zhang, H. B. Wu, X. W. Lou, Formation of Ni_xCo₃₋_xS₄ hollow nanoprisms with enhanced pseudocapacitive properties. *Angew. Chem. Int. Ed.* **53**, 3711–3714 (2014).

9. K. Bindumadhavan, S. K. Srivastava, MoS₂-MWCNT hybrids as a superior anode in lithium-ion batteries. *Chem. Commun.* **49**, 1823–1825 (2013).

10. L. F. Shen, L. Yu, H. B. Wu, X.-Y. Yu, X. Zhang, X. W. Lou, Formation of nickel cobalt sulfide ball-in-ball hollow spheres with enhanced electrochemical pseudocapacitive properties. *Nat. Commun.* **6**, 6694 (2015).

11. X.-Y. Yu, H. Hu, Y. Wang, H. Chen, X. W. Lou, Ultrathin MoS₂ nanosheets supported on N-doped carbon nanoboxes with enhanced lithium storage and electrocatalytic properties. *Angew. Chem. Int. Ed.* **54**, 7395–7398 (2015).

12. L. Zhang, H. B. Wu, Y. Yan, X. Wang, X. W. Lou, Hierarchical MoS₂ microboxes constructed by nanosheets with enhanced electrochemical properties for lithium storage and water splitting. *Energy Environ. Sci.* **7**, 3302–3306 (2014).

13. X. Xu, Z. Fan, X. Yu, S. Ding, D. Yu, X. W. Lou, A nanosheets-on-channel architecture constructed from MoS₂ and CMK-3 for high-capacity and long-cycle-life lithium storage. *Adv. Energy Mater.* **4**, 1400902 (2014).

14. C. Zhu, X. Mu, P. A. van Aken, Y. Yu, J. Maier, Single-layered ultrasmall nanoplates of MoS₂ embedded in carbon nanofibers with excellent electrochemical performance for lithium and sodium storage. *Angew. Chem. Int. Ed.* **126**, 2184–2188 (2014).

15. K. Chang, D. Geng, X. Li, J. Yang, Y. Tang, M. Cai, R. Li, X. Sun, Ultrathin MoS₂/nitrogen-doped graphene nanosheets with highly reversible lithium storage. *Adv. Energy Mater.* **3**, 839–844 (2013).

16. Y. Gong, S. Yang, Z. Liu, L. Ma, R. Vajtai, P. M. Ajayan, Graphene-network-backboned architectures for high-performance lithium storage. *Adv. Mater.* **25**, 3979–3984 (2013).

17. S. Ding, J. S. Chen, X. W. Lou, Glucose-assisted growth of MoS₂ nanosheets on CNT backbone for improved lithium storage properties. *Chem. Eur. J.* **17**, 13142–13145 (2011).

18. D. Kong, H. He, Q. Song, B. Wang, W. Lv, Q.-H. Yang, L. Zhi, Rational design of MoS₂@graphene nanocables: Towards high performance electrode materials for lithium ion batteries. *Energy Environ. Sci.* **7**, 3320–3325 (2014).

19. C. Zhang, Z. Wang, Z. Guo, X. W. Lou, Synthesis of MoS₂–C one-dimensional nanostructures with improved lithium storage properties. *ACS Appl. Mater. Interfaces* **4**, 3765–3768 (2012).

20. C. Zhang, H. B. Wu, Z. Guo, X. W. Lou, Facile synthesis of carbon-coated MoS₂ nanorods with enhanced lithium storage properties. *Electrochem. Commun.* **20**, 7–10 (2012).

21. J. J. Ge, H. Hou, Q. Li, M. J. Graham, A. Greiner, D. H. Reneker, F. W. Harris, S. Z. D. Cheng, Assembly of well-aligned multiwalled carbon nanotubes in confined polyacrylonitrile environments: Electrospun composite nanofiber sheets. *J. Am. Chem. Soc.* **126**, 15754–15761 (2004).

22. H. Hou, J. J. Ge, J. Zeng, Q. Li, D. H. Reneker, A. Greiner, S. Z. D. Cheng, Electrospun polyacrylonitrile nanofibers containing a high concentration of well-aligned multiwall carbon nanotubes. *Chem. Mater.* **17**, 967–973 (2005).

23. Y. Dror, W. Salalha, R. L. Khalfin, Y. Cohen, A. L. Yarin, E. Zussman, Carbon nanotubes embedded in oriented polymer nanofibers by electrospinning. *Langmuir* **19**, 7012–7020 (2003).

24. Y. M. Chen, X. Li, X. Zhou, H. Yao, H. Huang, Y.-W. Mai, L. Zhou, Hollow-tunneled graphitic carbon nanofibers through Ni-diffusion-induced graphitization as high-performance anode materials. *Energy Environ. Sci.* **7**, 2689–2696 (2014).

25. Y. Chen, Z. Lu, L. Zhou, Y.-W. Mai, H. Huang, Triple-coaxial electrospun amorphous carbon nanotubes with hollow graphitic carbon nanospheres for high-performance Li ion batteries. *Energy Environ. Sci.* **5**, 7898–7902 (2012).

26. W. Du, R. Liu, Y. Jiang, Q. Lu, Y. Fan, F. Gao, Facile synthesis of hollow Co₃O₄ boxes for high capacity supercapacitor. *J. Power Sources* **227**, 101–105 (2013).

27. Y. Wang, G. Xing, Z. J. Han, Y. Shi, J. I. Wong, Z. X. Huang, K. Ostrikov, H. Y. Yang, Prelithiation of onion-like carbon/MoS₂ nano-urchin anodes for high-performance rechargeable lithium ion batteries. *Nanoscale* **6**, 8884–8890 (2014).

28. X. Wang, G. Li, M. H. Seo, F. M. Hassan, M. A. Hoque, Z. Chen, Sulfur atoms bridging few-layered MoS₂ with S-doped graphene enable highly robust anode for lithium-ion batteries. *Adv. Energy Mater.* **5**, 1501106 (2015).

29. C. Zhu, X. Mu, P. A. van Aken, J. Maier, Y. Yu, Fast Li storage in MoS₂-graphene-carbon nanotube nanocomposites: Advantageous functional integration of 0D, 1D, and 2D nanostructures. *Adv. Energy Mater.* **5**, 1401170 (2015).

30. C. Zhao, J. Kong, X. Yao, X. Tang, Y. Dong, S. L. Phua, X. Lu, Thin MoS₂ nanoflakes encapsulated in carbon nanofibers as high-performance anodes for lithium-ion batteries. *ACS Appl. Mater. Interfaces* **6**, 6392–6398 (2014).

31. L. Ma, X. Zhou, L. Xu, X. Xu, L. Zhang, W. Chen, Chitosan-assisted fabrication of ultrathin MoS₂/graphene heterostructures for Li-ion battery with excellent electrochemical performance. *Electrochim. Acta* **167**, 39–47 (2015).

32. L. Yang, S. Wang, J. Mao, J. Deng, Q. Gao, Y. Tang, O. G. Schmidt, Hierarchical MoS₂/polyaniline nanowires with excellent electrochemical performance for lithium-ion batteries. *Adv. Mater.* **25**, 1180–1184 (2013).

33. J.-Z. Wang, L. Lu, M. Lotya, J. N. Coleman, S.-L. Chou, H.-K. Liu, A. I. Minett, J. Chen, Development of MoS₂–CNT composite thin film from layered MoS₂ for lithium batteries. *Adv. Energy Mater.* **3**, 798–805 (2013).

34. Y.-E. Miao, Y. Huang, L. Zhang, W. Fan, F. Lai, T. Liu, Electrospun porous carbon nanofiber@MoS₂ core/sheath fiber membranes as highly flexible and binder-free anodes for lithium-ion batteries. *Nanoscale* **7**, 11093–11101 (2015).

35. X. Zhou, L.-J. Wan, Y.-G. Guo, Synthesis of MoS₂ nanosheet–graphene nanosheet hybrid materials for stable lithium storage. *Chem. Commun.* **49**, 1838–1840 (2013).

36. L. Wang, Z. Xu, W. Wang, X. Bai, Atomic mechanism of dynamic electrochemical lithiation processes of MoS₂ nanosheets. *J. Am. Chem. Soc.* **136**, 6693–6697 (2014).

37. H. Hwang, H. Kim, J. Cho, MoS₂ nanoplates consisting of disordered graphene-like layers for high rate lithium battery anode materials. *Nano Lett.* **11**, 4826–4830 (2011).

38. J. Zhou, J. Qin, X. Zhang, C. Shi, E. Liu, J. Li, N. Zhao, C. He, 2D space-confined synthesis of few-layer MoS₂ anchored on carbon nanosheet for lithium-ion battery anode. *ACS Nano* **9**, 3837–3848 (2015).

39. H. Jiang, D. Ren, H. Wang, Y. Hu, S. Guo, H. Yuan, P. Hu, L. Zhang, C. Li, 2D monolayer MoS₂–carbon interoverlapped superstructure: Engineering ideal atomic interface for lithium ion storage. *Adv. Mater.* **27**, 3687–3695 (2015).

40. Y. Chen, Z. Lu, L. M. Zhou, Y.-W. Mai, H. T. Huang, In situ formation of hollow graphitic carbon nanospheres in electrospun amorphous carbon nanofibers for high-performance Li-based batteries. *Nanoscale* **4**, 6800–6805 (2012).

41. F. Zhou, S. Xin, H.-W. Liang, L.-T. Song, S.-H. Yu, Carbon nanofibers decorated with molybdenum disulfide nanosheets: Synergistic lithium storage and enhanced electrochemical performance. *Angew. Chem. Int. Ed.* **53**, 11552–11556 (2014).

42. J. R. Dahn, T. Zheng, Y. Liu, J. S. Xue, Mechanisms for lithium insertion in carbonacous materials. *Science* **270**, 590–593 (1995).

43. K. Kang, Y. S. Meng, J. Bréger, C. P. Grey, G. Ceder, Electrodes with high power and high capacity for rechargeable lithium batteries. *Science* **311**, 977–980 (2006).

44. X. Li, Y. Chen, L. Zhou, Y.-W. Mai, H. Huang, Exceptional electrochemical performance of porous TiO₂–carbon nanofibers for a lithium ion battery anode. *J. Mater. Chem. A* **2**, 3875–3880 (2014).

45. C. K. Chan, H. Peng, G. Liu, K. McIlwrath, X. F. Zhang, R. A. Huggins, Y. Cui, High-performance lithium battery anodes using silicon nanowires. *Nat. Nanotechnol.* **3**, 31–35 (2008).

Chen *et al. Sci. Adv.* 2016;2:e1600021   13 July 2016

7 of 8

Citation: Y. M. Chen, X. Y. Yu, Z. Li, U. Paik, X. W. Lou, Hierarchical MoS$_2$ tubular structures internally wired by carbon nanotubes as a highly stable anode material for lithium-ion batteries. *Sci. Adv.* **2**, e1600021 (2016).

Science Advances

Hierarchical MoS₂ tubular structures internally wired by carbon nanotubes as a highly stable anode material for lithium-ion batteries

Yu Ming Chen, Xin Yao Yu, Zhen Li, Ungyu Paik and Xiong Wen (David) Lou

ARTICLE TOOLS	http://advances.sciencemag.org/content/2/7/e1600021
SUPPLEMENTARY MATERIALS	http://advances.sciencemag.org/content/suppl/2016/07/11/2.7.e1600021.DC1
REFERENCES	This article cites 45 articles, 2 of which you can access for free http://advances.sciencemag.org/content/2/7/e1600021#BIBL
PERMISSIONS	http://www.sciencemag.org/help/reprints-and-permissions

Use of this article is subject to the Terms of Service